Innovative Food Science and Emerging Technologies 97 (2024) 103789

Contents lists available at ScienceDirect

Innovative Food Science and Emerging Technologies

journal homepage: www.elsevier.com/locate/ifset

# Improved lifetime of a pulsed electric field (PEF) system-using laser induced surface oxidation

Mark Swayne [a,b,*], Gopinath Perumal [a,b], Dilli Babu Padmanaban [c], Davide Mariotti [d], Dermot Brabazon [a,b]

[a] I-Form Advanced Manufacturing Centre Research, Dublin City University, Glasnevin, Dublin 9, Ireland
[b] EPSRC & SFI Centre for Doctoral Training (CDT) in Advanced Metallic Systems, School of Mechanical & Manufacturing Engineering, Dublin City University, Glasnevin, Dublin 9, Ireland
[c] Plasma Science and Nanoscale Engineering Group, School of Engineering, Ulster University, York Street, Belfast, Northern Ireland, United Kingdom
[d] University of Strathclyde, Department of Design, Manufacturing & Engineering Management, Glasgow, Scotland, United Kingdom

ARTICLE INFO

*Keywords:*
PEF
Laser induced oxidation
Waveform analysis
Metal Ion reduction

ABSTRACT

In this research, we explore the possibility and effectiveness of using laser-induced surface oxidation methods to enhance the durability and effectiveness of PEF (Pulsed Electric Field) systems. Despite advantages over thermal pasteurisation, PEF faces challenges like electrode corrosion and biofouling, hindering its adoption. This research introduces laser-induced oxidation to mitigate metal ion release during PEF, directly targeting electrode alteration. Our examination adopts a comprehensive method, integrating Design of Experiments (DoE) parameter sets for PEF trials, morphological analysis, evaluation of metal ion release via Inductively Coupled Plasma Quadrupole Mass Spectrometry (ICP-QMS), waveform capture utilizing a Data Acquisition (DAQ) system, electrochemical assessment via impedance spectroscopy, and examination of oxide layer composition employing X-ray photoelectron spectroscopy. Pulse waveform characteristics shows the intricate relationship between PEF processing parameters with metal ion release, alongside XPS analysis providing insights into surface chemistry. Optimized results show a three-fold reduction in metal ion release post-PEF, with laser-treated samples outperforming untreated stainless steel due to selective surface chemistry alteration, notably an increased Cr/Fe ratio, reducing harmful elements. This study highlights laser-induced oxidation as a practical solution for enhancing PEF electrode performance and reducing metal ion release, addressing key challenges in PEF technology. It advances sustainable food processing, promising extended PEF system lifespan while maintaining efficiency and product quality.

## 1. Introduction

Concerns about the long-term viability of the world's food supply are nothing new for the food industries. It is critical for the food manufacturing industry to develop processing technologies that can maintain and improve the nutritional value of foods while also producing bio-accessible compounds. The food industry is investing more resources in nonthermal processing technologies such as pulsed electric fields (PEF), ultrasound, high hydrostatic pressure, pulsed light, and ultraviolet radiation (Aadil et al., 2015, 2018; Aadil et al., 2020; Li & Farid, 2016). Cohn and Mendelsohn published their findings on sterilisation by passing a DC-current through a nutrient solution in 1879. In recent decades, there has been a surge of interest in Pulsed Electric Field technology (PEF), which is a viable alternative for thermal food pasteurisation (Tylewicz, 2020). PEF is a method of food preservation that involves exposing the food to electric field pulses with typical field strengths of 2–5 kV/mm and pulse durations of 1-1000 μs. The most significant advantages of PEF pasteurisation over thermal pasteurisation are the preservation of fresh-like characteristics and the reduction of processing energy required. By subjecting food products to short, high-voltage electrical pulses, PEF effectively deactivates microorganisms and enzymes while minimizing the detrimental effects on food quality. Under the influence of this external electrical field, biological membranes are punctured by the formation of hydrophilic pores and the forced opening of protein channels (Gášková et al., 1996; Tsong, 1991). Once pores of 0.5 nm radius are formed, they may expand as a result of

* Corresponding author at: I-Form Advanced Manufacturing Centre Research, Dublin City University, Glasnevin, Dublin 9, Ireland.
*E-mail address:* Mark.swayne2@mail.dcu.ie (M. Swayne).

https://doi.org/10.1016/j.ifset.2024.103789
Received 28 May 2024; Received in revised form 8 August 2024; Accepted 13 August 2024
Available online 15 August 2024

the applied electric field, disrupting the flow of material into and out of the cell (Sale & Hamilton, 1967).

The loss of membrane integrity causes cell contents to diffuse into their surroundings, resulting in the death of the living cell, a process known as irreversible electroporation (Gavahian et al., 2018). Multiple studies have demonstrated that PEF successfully decreases the initial microbial load in liquid food products during pasteurisation, with minimal loss of nutrients and flavour (Gavahian et al., 2018; Sale & Hamilton, 1967; Yogesh, 2016; Zhang et al., 2023; Zhao et al., 2008). Despite these promising results, a full transition from thermal to PEF has not occurred in industry due to some underlining issues experienced during the process. These are first, a short life span of the electrodes themselves, which must be replaced frequently due to the high corrosion that occurs; and second, biofouling caused by the food product inside the system (Roodenburg et al., 2005a). Thus, the practical implementation of PEF systems faces challenges related to electrode durability and maintenance, particularly concerning electrode degradation and fouling over prolonged usage. The electrode biofouling is due to be caused by the electrophoretic concentration of charged molecules within a boundary layer of food product that is adjacent to the treatment electrode. This agglomeration of the fouling agent on the electrode(s) during extended processing periods can result in arcing and reduced flow inside the system, further reducing the system's lifetime (Pataro & Ferrari, 2022).

During food product treatment in a PEF system, the electrodes directly contact the liquid media, the current that flows in the electrode will consist of free electrons and in the liquid of charged particles. At the electrode-electrolyte interface, an electrical double layer forms, resembling a capacitor. Application of an external voltage increases this double layer's voltage until it reaches the threshold voltage (Uth), causing two independent electrochemical half-cell redox reactions occur in order to preserve charge conservations. This corrosion not only reduces electrode lifespan but also raises the risk of food contamination (Roodenburg et al., 2005b). Hazardous byproducts can form inside the reaction chamber, such as chloride gas ($Cl_2$) which is produced at the anode and can react with the water molecules producing hypochloric acid (Rodaitė-Riševičienė et al., 2014). Roodenburg et al. studied pulse shape effects on metal release from electrode surfaces in a NaCl solution, identifying three pulse topologies. (Roodenburg et al., 2005a). Their findings showed a significant reduction in metal release when pulses contained both positive and negative waveform portions, with a notable 29-fold increase in iron concentration observed after switching from an exponential decaying pulse to an oscillatory decaying pulse. Various factors, including chamber design (Matra et al., 2020), and electrode material (Gad et al., 2014; Góngora-Nieto et al., 2002; Samaranayake & Sastry, 2005; Tanino et al., 2020), electrical parameters such as peak voltage, total specific energy input, polarity, and pulse duration (Gad et al., 2014; Kotnik et al., 2001), as well as the composition and chemical– physical properties of the treated medium (Gad et al., 2014; Meneses et al., 2011; Nowosad et al., 2021; Roodenburg et al., 2005a), have been studied for their influence on metal release from electrodes in PEF systems. While much research has focused on optimizing process conditions, little attention has been given to surface anticorrosion treatments. Although some studies have explored coating electrodes with conductive-plastic films (Roodenburg et al., 2010) and ceramic-coatings (Ashokkumar & Adler-Nissen, 2011), these methods may introduce new compounds into the solution, potentially disrupting industrial process conditions.

One promising approach to address these challenges is the utilization of laser-induced surface oxidation techniques to enhance the lifetime and performance of PEF systems. Laser induced oxidation is an almost instantaneous process due to the rapid heating and cooling causes a non-equilibrium oxidation process. By applying controlled laser energy to electrode surfaces, surface properties can be modified to improve corrosion resistance, reduce fouling, and enhance electrical conductivity. This highly precise technique allows us to fine-tune the thickness and chemical composition of the oxide film, as observed in a study Cui et al. (2014) who derived a thermokinetic model to describe the composition of the film produced (Cui et al., 2014). The Gaussian energy distribution of laser pulses leads to non-homogeneous morphology, with peak power concentrated at the center (Alda, 2003). This results in a duplex oxide formation, with chromium oxide ($Cr_2O_3$) concentration doubling on the surface due to its higher affinity for the chemisorbed oxygen (Cui et al., 2014). Nevertheless, due to the higher temperature at the center and the higher diffusion rate of Fe inside the oxide layer, $Fe_2O_3$ becomes present at the surface of the stainless steel, altering the Cr/Fe ratio. These results were both consistent with previous literature results (Z. L. Li et al., 2009; Lu et al., 2017). Łęcka et al. (2016) found that varying surface energy affects corrosion resistance, with an initial large increase reaching a maximum at lower fluences, followed by a sharp decrease to the unprocessed value, correlating with changes in the Cr/Fe ratio (Łęcka et al., 2016). These findings align with previous research by Li and Lu, indicating the critical role of surface chemistry in corrosion resistance (Cui et al., 2014; Li et al., 2009).

**Table 1**
Parameter set for laser processed PEF electrodes.

| Sample | Power (%) | Frequency (Hz) | Scan Speed (mm/s) | Hatching Distance (um) |
|---|---|---|---|---|
| S-A | 80 | 100 | 450 | 8 |
| S-B | 80 | 100 | 250 | 15 |
| S-C | 80 | 100 | 450 | 1 |

In this research, we explore the possibility and effectiveness of using laser-induced surface oxidation methods to enhance the durability and effectiveness of PEF (Pulsed Electric Field) systems. Our investigation takes a thorough approach, incorporating Design of Experiments (DoE) parameter sets for PEF experiments, morphological analysis, assessment of metal ion release using Inductively Coupled Plasma Quadrupole Mass Spectrometry (ICP-QMS), waveform collection facilitated by a Data Acquisition (DAQ) system, electrochemical examination through impedance spectroscopy, and analysis of oxide layer composition using X-ray photoelectron spectroscopy (XPS). Our aim is to understand the mechanisms behind the observed improvements comprehensively. Additionally, we seek to assess the practical implications and


**Fig. 1.** Elea pulsed electric field system, with schematic of PEF test layout.

**Table 2**
Possible parameter for the commercial used Elea PEF pilot plant.

| Parameter | Range | Intervals |
|---|---|---|
| Electrode Voltage | 4–24 kV | 1 kV |
| Pulse Count | 1–10,000 Pulses | 1 Pulse |
| Frequency | 1–500 Hz | 1 Hz |
| Pulse Width | 4–7 μs | 1 μs |

**Table 3**
DOE 1 parameter set for pulsed electric field experiment.

| Run | Voltage (kV) | Frequency (Hz) | Pulse width (μs) |
|---|---|---|---|
| 1 | 16 | 35 | 7 |
| 2 | 16 | 35 | 4 |
| 3 | 24 | 20 | 6 |
| 4 | 24 | 5 | 4 |
| 5 | 20 | 20 | 6 |
| 6 | 20 | 20 | 7 |
| 7 | 20 | 5 | 6 |
| 8 | 20 | 20 | 6 |
| 9 | 20 | 20 | 6 |
| 10 | 24 | 35 | 7 |
| 11 | 20 | 20 | 4 |
| 12 | 24 | 5 | 7 |
| 13 | 16 | 20 | 6 |
| 14 | 20 | 20 | 6 |
| 15 | 16 | 5 | 7 |
| 16 | 20 | 20 | 6 |
| 17 | 24 | 35 | 4 |
| 18 | 20 | 35 | 6 |
| 19 | 20 | 20 | 6 |
| 20 | 16 | 5 | 4 |
| **Pulses = 10,000** | | | |
| **Solution = 20 mM NaCl** | | | |
| **1 L solution** | | | |

relationships among parameters relevant to large-scale PEF processing. By clarifying the connection between laser-induced surface alterations and PEF system performance, this study contributes to the advancement and application of PEF technology in the food industry, ultimately aiding the development of more sustainable and efficient food processing methods.

## 2. Method

### 2.1. Sample preparation

Sheets of stainless steel measuring 100 × 200 × 0.8 mm were purchased from Impact Ireland (Metals) Limited, Ireland. All samples were cleaned using deionized water and then ethanol. The surface of the steel was then uniformly sandblasted to increase the average area surface roughness to 3.9 μm $S_a$ to enhance laser absorption (Ahmed Obeidi et al., 2019). Table 1 depicts the list of parameters that were selected for laser processing and the total areal surface energy used to produce them (Swayne et al., 2024). These results performed the best and worst in terms of general and pitting corrosion performance evaluated using electrochemical cyclic polarization tests done on two preliminary design of experiment studies, P1 and P2. Afterwards, the bottom 25 mm of each sample was laser processed in the same manner as described above; however, due to the larger size of the samples and the small processing area of the laser (75 × 75 mm), realignment and stitching of the laser processing were required. Fig. 1 shows the PEF system (Elea pilot plant) used for the investigation.

### 2.2. PEF processing

The PEF pilot solid was supplied by Elea technology, the system was set up in batch processing mode, using a 30 $cm^3$ chamber. To determine the effect of PEF parameters on the amount of metal released during pulsed processing, a central composite face-centered DOE design was utilized. A 20-run design with 15 distinct parameter sets and five repetitions of the central point are utilized. The investigated parameters included the pulse width, the frequency, and the voltage seen in Table 2.

As the pilot plant is evaluating a low field strength system (1 kV/cm) due to its large electrode gap, the amount of material removed from the electrode surface is comparably low. Therefore, longer run times were required to bring the metal ion concentration above the detectable limit; therefore, a constant value of 10,000 pulses was used for each experimental run in the DOE 1.

The system is equipped with additional safety features to protect both the machine and the user because they are designed for commercial use. This restricts the amount of current that can flow through the machine; as a result, we can only use a lower pulse count below 10,000 pulse range, as higher frequencies will cause faster heating of the electrolyte, allowing the current to exceed the warning value and causing a voltage drop as a safety response. This consideration led to the selection of the maximum frequency of 35 Hz. For similar reasons, the conductivity of the electrolyte can also cause the current threshold to be reached; therefore, a 20 mM NaCl solution was selected for the experiment which has an electrical conductivity of 0.22 S/m. The DOE 1 parameters are displayed in Table 3.

Prior to PEF processing, the surface of the batch cell and unprocessed electrodes were cleaned with DI water and acetone to remove any contaminants. The electrode was attached to the batch cell using clamps. The batch cell was inserted into the PEF system and its electrical contact was attached. The cell was filled with 1 L of electrolyte (NaCl), and the system was sealed. For DOE 1, a sample was collected every 10,000 pulses using a 10 mL pipette and a 50 mL sterilized solution holder from 5 fixed locations inside the reactor vessel, one in the center and four at each corner, in order to reduce the effect of solution inhomogeneity. After the total number of pulses, the system was cleaned and each run utilized fresh electrodes and electrolyte. After each run, the maximum voltage, current, and total energy supplied to the system were recorded from the pilot plant display.

### 2.3. Laser processing

The sand blasted sample was cleaned with acetone and ethanol and sonicated for 15 min to remove any contaminants or excess sand from the surface then allowed to dry for 5 min on the laser stage. The laser system used consisted of a 3.5 W max power 1064 nm Q-switched, diode-pumped solid-state neodymium-yttrium aluminium garnet laser (BrightSolutions 1064 WEDGE HF). A 2D scanning galvanometer (Raylase SS-12) was used to raster the beam in the xy-plane, and a movable z-stage (PI M-404 4PD) was used to control the position of the sample. The beam was focused on the surface of the samples which lies 34.03 mm below the Galvo lens this produces a spot size of 100 μm. The samples where then processed using fixed parameters of a bidirectional hatching strategy.

### 2.4. PEF processing of the laser processed electrodes

The set of laser processed parameters used for PEF pulsed processing can be seen in Table 1. The laser processed electrode where PEF processed using fixed machine parameter of 24 kV, 5 Hz, 7 μs, 30,000 pulses and 1 L solution. Each electrode was repeated three times with samples being collected every 10,000 pulses.

### 2.5. Metal Ion concentration measurements

The elements of interest for this analysis where, Iron, Chromium, Nickel, Manganese and Molybdenum. Calibration standards were made volumetrically using a 100 mg/L TraceCERT® Sigma-Aldrich multi-element standard and a 0.3 M $HNO_3$ stock solution. The acid stock

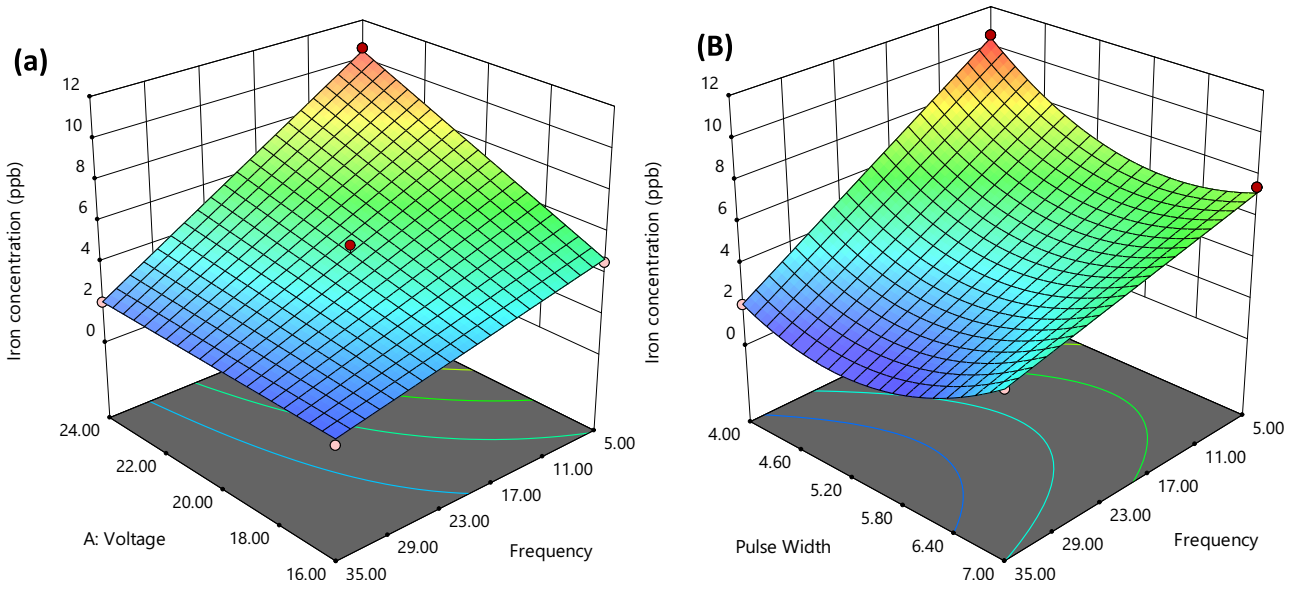


**Fig. 2.** (A) Response surface for the iron corrosion inside a PEF system with constant pulse width of 4 μs. (b) Response surface for the iron corrosion inside a PEF system with constant voltage of 24kv.

solution was made from Optima grade concentrated $HNO_3$ (68% *w*/w; Fisher Scientific trace metal grade acids) and purified water with a resistivity ≥18.2 MΩ cm from a Milli-Q system (Merck Millipore). The concentrations of the calibrants were between 0.1 and 500 μg/L. All calibration solutions and blanks were doped with a Leehman Labs (Teledyne) 100 ppm Gallium and a Perkin Elmer 1000 mg/L Yttrium standard solutions to obtain a consistent concentration of 50 μg/L (for both Ga and Y) for all solutions. Samples were diluted by a factor of 10 to lower the electrolyte (NaCl) concentration. All measurements were conducted using a Perkin Elmer NexION 350D Inductively Coupled Plasma Quadrupole Mass Spectrometer (ICP-QMS) under Kinetic Discriminator (KED) mode for the element masses 52Cr, 55Mn, 56Fe,60Ni and under Standard mode for the element mass 95Mo at the London Metallomics Facility, King's College London.

The introduction system to the instrument employed a Cetac ASX-100 auto sampler coupled to a SeaSpray glass nebulizer fitted to a quartz cyclonic spray chamber. Argon plasma flow and nebulizer gas flow rates were 18 L/min and 0.93 L/min, respectively. Quality control of ICP-QMS measurements was ensured through repeat measurements of blanks; a calibrant and a certified reference material (trace metal drinking water from High Purity Standards –CRM-TMDW-100). Sample measurements in counts per second (cps) were normalized to the Ga and the Y internal standards to account for both instrument drift and matrix effects. Sample and standard intensities were subsequently blank corrected by removing the average isotopic intensity (cps) of repeat blank measurements. The corrected isotopic intensity was converted to concentration measurements by applying a regression model from the calibration analysis.

### 2.6. Waveform acquisition

Waveform acquisition was performed using LabVIEW Software and the NI DAQ system. The voltage and current were directly measured from the output port on the pilot plant. Both the current and voltage signals were expressed as a damped voltage value, so a multiplier of 24,000 and 1000 were applied to the recorded voltage and current values respectively to acquire the real values. An acquisition rate of 125,000 was used for both input signals. The recorded data was then analysed in python to acquire the voltage and current change during processing, and the effect of the parameters on the phases of the current and voltage to each other.

### 2.7. Surface characterization analysis

X-ray photoelectron spectroscopy (XPS) was performed on laser processed 316 L SS samples using ESCALAB Xi+ spectrometer microprobe (Thermo Fisher Scientific) with a focussed monochromatic Al Kα X-ray source ($h\nu = 1486.6$ eV, spot area of 650 μm × 650 μm) operating at a power of 225 W (15 kV and 15 mA) and the photoelectrons were collected using a 180° double-focusing hemispherical analyser with a dual detector system. The spectrometer was prior calibrated with sputter cleaned references such as Au, Ag and Cu supplied by Thermo Fisher scientific. The base pressure of analysis chamber was always maintained $<5 \times 10^{-9}$ mbar, which increased up to $\sim 5 \times 10^{-7}$ mbar during measurement along with charge neutraliser (flood gun) operated at 100 μA emission current. XPS and sub-surface chemical composition were performed using soft cluster clean and monoatomic depth profiling using Ar gas. In cluster clean, sample surface of raster size 3.25 mm was exposed to Ar clusters of size 1000, energy at 4 keV for 30 s. In all these cases, survey scan spectra were recorded with parameters of step size 1 eV, pass energy 150 eV and narrow core shell high resolutions scans are done at step size of 0.1 eV, pass energy of 20 eV respectively. Casa XPS software was used to analyse the results for elemental composition and chemical oxidations states of all elements of interest. 2p 3/2 peak was taken into account for the composition analysis of chromium, and Iron while for oxygen the 2 s singlet peak was used and for molybdenum both the 3p 5/2 and 3p 3/2 peaks were taken into account. The location of the peaks was identified with wide literature seen in supplementary S1. Further, the high-resolution spectra were analysed thoroughly by deconvoluting using asymmetric Lorentzian peak fitting function with Shirley background functions The sensitivity factor and peak position can be seen in supplementary S1.

## 3. Results

### 3.1. Effect of altering parameters on the metal ion concentration

The ANOVA analysis reveals that all three processing parameters exert influence over the iron ion concentration, demonstrating a quadratic relationship among them. Voltage and pulse width positively influence the concentration, whereas frequency has a negative impact. Frequency exerts the most significant effect on system corrosion, followed by voltage, with pulse width having the least impact. This is

**Table 4**
Electrochemical impedance spectroscopy results for S-A, S-C and unprocessed.

| Sample | Rtotal (k ohm/cm) | Rp | $C_{dl}$ (μS $s^a/cm^2$) | Ri | CPEi | Ro | CPEo | Rpore | CPEpore | α |
|---|---|---|---|---|---|---|---|---|---|---|
| Unprocessed | 384,736 | 375,800 | 757.5 | 8936 | 5475 | – | – | – | – | 0.787 |
| S-A | 586,015 | 547,200 | 473.4 | 15 | 3592 | 38,800 | 773.2 | – | – | 0.921 |
| S-C | 37,362.85 | 7639 | 3599 | 6.75 | 2604 | 417.1 | 4355 | 29,300 | 1337 | 0.822 |

evident from the two highest results of 10.56 and 7.48 ppb, both associated with high voltage (24 kV) and the lowest frequency (5 Hz), whereas the three lowest results of 1.54, 2.00, and 2.04 ppb are all associated to the highest frequency of 35 Hz. These results indicate two significant two-factor interactions. Firstly, a negative relationship is observed between voltage and frequency, where at higher voltages, the impact of frequency on iron concentration becomes more pronounced. Specifically, with increasing voltage, the frequency-iron concentration graph exhibits a steeper trend. Secondly, a positive two-factor interaction is noted between frequency and pulse width, albeit with less strength compared to the voltage-frequency interaction.

From the ANOVA analysis, a quadratic model was designed to describe the iron concentration of possible runs using the three starting parameter and can be described by the Eq. (1). With V being the voltage, W being the pulse width and F being the frequency:

$$\mathrm{Fe} = 15.012 + 1.15\,\mathrm{V} + 0.0325\mathrm{F} - 9.33\,\mathrm{W} - 0.0227\mathrm{VF} - 0.0814\mathrm{VW} + 0.058\mathrm{FW} + 0.901\mathrm{W}^2 \quad (1)$$

Visual representation of the model can be seen in Fig. 2. To minimize the Fe concentration in the system the lowest pulse width and voltages should be used, alongside with the highest frequency, the model used to describe shows quite high correlation with an $R^2$ value of 0.8970.

### 3.2. Total energy input

The entire energy of each portion of the 10,000-pulse run was recorded from the pilot plant's readout and summed together. Using Design Expert, the findings were analysed, and a model with a very high correlation coefficient ($R^2$) of 0.9973 was developed. When the voltage and pulse width are varied, this model exhibits a high positive dependence, whereas the applied frequency has a minor dependence. The results show that for when all other factors stay constant the total energy varies almost linearly with voltage. The equation derived from the ANOVA model is seen in Eq. (2).

$$\text{Total Energy} = 238,100 + 119,900\,\mathrm{V} + 11767\mathrm{F} + 103,600\,\mathrm{W} + 60831\mathrm{VW} + 10639\mathrm{FW} \quad (2)$$

### 3.3. Effect of processes parameters on the wave formation

Waveform graphs of the voltage and current were recorded using LabVIEW software. It can be seen that both the voltage and current form as mono-polar square wave pulses. It can be seen Fig. 4A that there is a linear increase in the current as the run continues, while the voltage stays relatively constant, this rise in current is due to the increase in solution temperature due to the applied energy from the pulses. A secondary reason for this increase is due to the segregation of ions in the solution due to their electrostatic interaction with the anode or cathode. The rate of increase of the current is heavily influenced by the frequency due to the high total energy applied.

Fig. 4C and D show the variation of the waveform with altering frequency, graph C is run at 100 Hz while D is running at 1 Hz. These graphs show that the phase of the current and voltage to each other can alter with frequency from being completely in phase at low hertz and almost fully out of phase at higher hertz. This alters the power of each pulse being ~10 kW for high frequency and ~ 1500 kW for low frequency. This alteration in the peak pulse power can explain for high corrosion rate seen at the lower frequencies.

**Table 5**
Surface composition of the laser processed samples, including the Cr/Fe ratio.

| Sample | Fe (at. %) | Cr (at. %) | Mn (at. %) | Ni (at. %) | O (at. %) | Cr/Fe |
|---|---|---|---|---|---|---|
| S-A | 6.01 | 21.67 | 3.04 | 4.75 | 64.52 | 3.61 |
| S-B | 9.24 | 21.17 | 4.38 | 0.00 | 65.21 | 2.63 |
| S-C | 23.12 | 5.85 | 2.29 | 9.79 | 58.95 | 0.25 |
| Unprocessed | 14.01 | 9.92 | 0.61 | 6.37 | 69.09 | 0.71 |

### 3.4. Electrochemical impedance spectroscopy (EIS)

Fig. 5 depicts the Bode plots obtained from the EIS measurements conducted in a 0.5 M NaCl solution at the Open Circuit Potential (OCP) for S-A, S-C, and an unprocessed sample. These measurements were conducted within the frequency range of 0–100 Hz, typical.

for the PEF system. Upon comparison of impedance values, it was observed that S-A exhibited significantly lower impedance than the unprocessed sample, while S-C displayed notably higher impedance than both counterparts. This trend is graphically depicted in Fig. 5. The phase angle versus frequency plot for all samples, as shown in Fig. 5, revealed a broad peak within the mid-frequency range, indicating the capacitive behaviour of the system. This capacitive response originates from charge transfer phenomena and the formation of double-layer capacitance at the metal/electrolyte interface. The diameter of the capacitive loop correlates with the charge transfer resistance ($R_p$), where higher $R_p$ values signify reduced dissolution rates and, consequently, heightened corrosion resistance. Notably, S-A exhibited the most substantial phase shift across the entire frequency spectrum, indicating superior capacitive characteristics.

Each of the three samples depicted distinctive Bode plots, indicative of their respective surface characteristics. All samples manifested multiple time constants. Specifically, the unprocessed sample was modelled with an Equivalent Electrical Circuit (EEC) comprising two time constants in series, attributed to the oxide layer and surface roughness resulting from sandblasting. S-A extended this unprocessed specimen circuit to encompass a third time constant, reflecting the formation of a multilayer oxide. Similarly, S-C exhibited the same three time constants as S-A, with an additional fourth time constant in parallel to accommodate the influence of porosity/cracks in the outer passive film. The EECs representing the unprocessed steel and both processed samples are illustrated in Fig. 5 as insets.

In this context, $C_{dl}$ and $R_p$ represent the electrochemical double-layer capacitance and charge transfer resistance, respectively, for the high-frequency portion of the spectrum. $CPE_i$ and $R_i$ represent the corresponding elements for the inner oxide layer properties, while $CPE_o$ and $R_o$ represent the outer oxide layer. $CPE_{pore}$ and $R_{pore}$ represent the pore capacitance and resistance, respectively. CPE, a frequency-dependent constant phase element with exponent α, was utilized instead of pure capacitance to accommodate surface in homogeneities. The values of different elements of the electrochemical equivalent circuit are summarized in Table 4.

Furthermore, $R_{total}$ represents the overall resistance for both processed and unprocessed specimens (refer to Table 4). S-A demonstrated the highest total resistance, followed by the unprocessed sample, and then S-C. It is noteworthy that the charge transfer resistance exhibited by

S-A was notably higher compared to the other two specimens. Additionally, the α value for both processed samples was higher, indicating a shift towards a more capacitive nature, rising from 0.787 for the unprocessed sample to 0.921 for S-A.

### 3.5. X-ray photoelectron spectroscopy (XPS) analysis

Based on the XPS analysis of the laser-treated samples, it is apparent that the oxide film primarily consists of iron and chromium oxides, with minor traces of other alloying elements (Fig. 6). However, the composition of these films differs among the three treated electrodes (Table 5). Particularly, S-A and S-B exhibit closely resembling compositions, characterized by notably high Cr/Fe ratios. In contrast, S-C displays elevated concentrations of additional alloying elements, predominantly nickel oxides.

For a thorough analysis, please refer to the high-resolution XPS scans presented in Fig. 6. Additionally, supplementary information (S1) provides valuable insights into sensitivity factors, reference peaks, and experimentally captured peak positions.

#### 3.5.1. Fe 2p spectral analysis

Upon examination of the Fe 2p spectra (Fig. 6g-i), four prominent peaks emerge at binding energy levels of 710–711, 724–725, 715–716, and 729 eV, corresponding to Fe 2p3/2 and Fe 2p1/2 states. Notably, the peaks at 716 eV and 729 eV are identified as satellite peaks, indicative of Fe (III) oxides, specifically $Fe_2O_3$. Additionally, in cases of lower energy runs, such as S-A and S-B, an additional peak at approximately 706 eV is discernible, signifying incomplete oxidation and the presence of metallic Fe on the surface. S-A and S-B exhibit a reduction in iron relative content, decreasing to 6.01% and 9.24% respectively from the unprocessed value of 14.01%, while S-C demonstrates an increase in Fe relative content up to 23.12%.

#### 3.5.2. Cr 2p spectral analysis

The Cr 2p spectra (Fig. 6a-c) reveal three primary peaks at binding energies around 577 eV, 580 eV, and 587 eV corresponding to Cr 2p3/2 for Cr(III) oxide, Cr 2p3/2 for Cr(VI) oxide, and Cr 2p1/2 for both oxides, respectively. The lower areal energy samples S-A and S-B exhibit only the Cr(III) component while the S-C sample has both Cr(III) and Cr (VI) components in a ratio of 89% to 11% respectively. The total Cr content for S-A and S-C is significantly increased to 21.67% for S-A and 21.17% for S-B, compared to the unprocessed value of 9.92% while S-C shows a decreased Cr content down to 5.85%.

#### 3.5.3. Mn 2p spectral analysis

The spectrum (Fig. 6d) reveals the presence of 2 major peaks on at 641.5 eV and one at 653.4 eV with a satellite present at 645.5 eV these peaks correspond to the Mn 2p3/2 and Mn 2p1/2 for Mn(0) respectfully. All 3 processed samples experience the same oxide type, with MnO being the main oxide produced this is evented by the satellite peak present and the delta E gap of 5.8 eV seen in the Mn 3 s peak. Furthermore, all three laser-processed samples demonstrate elevated relative concentrations compared to the unprocessed sample, which stands at 0.61%. Among them, S-B experiences the most significant increase, reaching up to 4.38%.

#### 3.5.4. Ni 2p spectral analysis

Examination of the Ni 2p spectra (Fig. 6f) unveils two prominent peaks at 855.4 eV, accompanied by a peak at 873.0 eV, with satellite peaks observed at 861.7 eV and 880 eV. These peaks correspond to the Ni(II) state, characteristic of the nickel hydroxide compound $Ni(OH)_2$. Notably, S-C exhibits an increased Ni content of 9.79% on the surface compared to the unprocessed steel, which stands at 6.37%. Conversely, S-A showcases a reduction in Ni content to 4.75%, while S-B demonstrates complete elimination of Ni content from the surface.

### 3.6. Effect of laser processing on the metal realised

As can be seen in Fig. 7(a) the total metal released from the electrodes was reduced dramatically for the electrodes processed with lower number of pulses with respect to the unprocessed sample total ion released (dashed black line) the total elemental concentration only exceeding the unprocessed electrode after 3 times the pulse count on the electrodes. The total ion concentration is also similar for the three electrodes, with S-C ion total concentration being slightly higher. S-A shows a 4-fold decrease in total ion concentration after 10,000 pulses. However, the make-up of the ion concentration from the different elements varies substantially from the general trend. It can be seen that for S-C, after 10,000 pulses, the individual elemental ion concentrations are all lower than the corresponding concentrations of the unprocessed stainless steel (SS) for any element after 10,000 pulses. While for S-A and S-B, the Cr concentration exceeds substantially the Cr concentration of unprocessed SS after 10,000 pulses. On the other hand, for S-A and S-B, the ion concentration of Ni has decreased drastically with respect to the unprocessed electrode, even after 30,000 pulses. Ni ion concentration for S-C however, exceeds the concentration of the unprocessed sample after 30,000 pulses. Iron and nickel make up the majority of the elements measured inside the solution.

### 3.7. Morphology analysis

SEM images of the unprocessed sample as well as the laser processed samples S-A and S-C are shown in Fig. 8, providing a visual insight into the effects of laser processing on their surface morphology. Inspection of the unprocessed sample unveils an initial morphology characterized by pronounced surface irregularities and a heterogeneous morphology characterized by the presence of an array of defects (cracks and pinholes). Delving into the morphology analysis depicted in Fig. 8B, it becomes apparent that the lower areal energy laser processing methodology reduces a multitude of surface defects stemming from the intricate interplay of oxide growth, and the laser remelting and solidification process. Particularly noteworthy is the revelation within the higher areal energy processed samples (Fig. 8c), where the emergence of defects within the oxide film, such as cracks and a markedly porous structure, due to the higher thermal stresses applied, underscores the important interplay between processing parameters and resultant surface characteristics. The phenomenon of oxide growth creates significant alterations in the optical properties of the surface, precipitating observable changes in surface colour owing to the intricate mechanism of thin film interference triggered by the growth of oxide thin films.

The examination of post-PEF processed electrodes unveils notable disparities, with conspicuous evidence of oxide removal evident across all electrodes although to varying degrees. S-A shows the least amount of oxide removal, surpassing both the blank and S-C counterparts. The blank sample, while exhibiting a reduced proportion of oxide removal compared to its S-C, displays individual spots characterized by larger and deeper impressions, indicative of the onset of localized corrosion phenomena. S-C experiences the most amount of oxide removal evident by the laser proportions of dark spots present on the surface. It is also event that the majority of oxide removal is seen in the troughs of the surface morphology.

## 4. Discussion

A variety of methodologies have been discussed in the literature that are capable of reducing metal ion release during the PEF process optimisation. However, we have proposed here the first practical implementation of a method that focused on diminishing ion release through the modification of the PEF electrode surface.

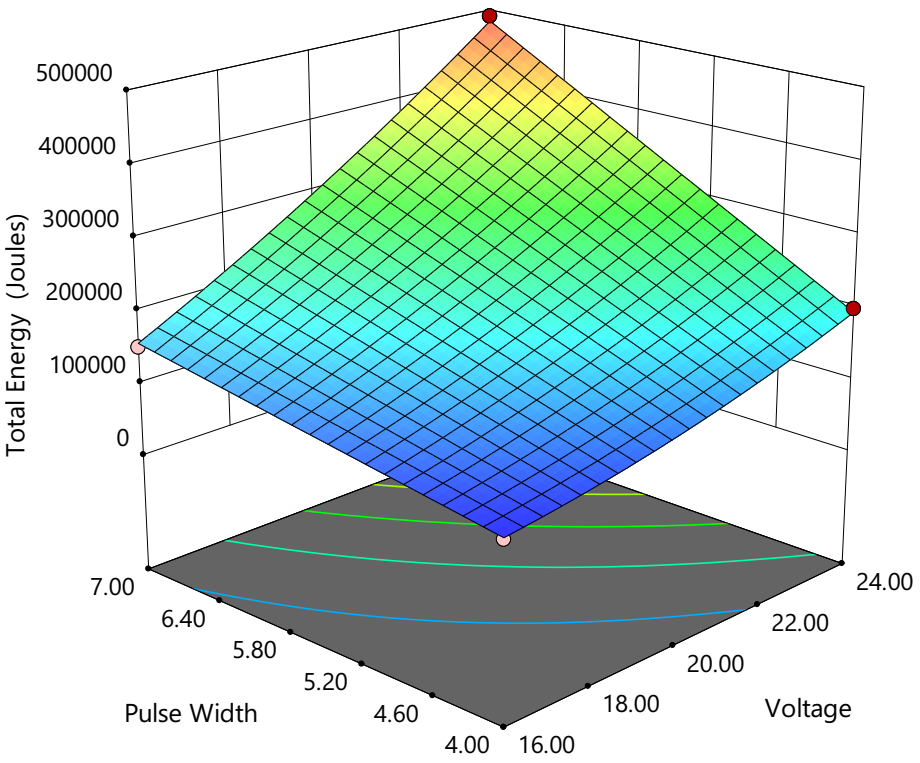


**Fig. 3.** Response surface for the total energy inside a PEF at constant frequency of 35 Hz.

### 4.1. Iron concentration

Since the waveform used by the Elea PEF pilot plant is a monopolar square wave pulse, it causes a nearly instantaneous rise in voltage to its peak value, where it is held for an extended period of time above the threshold voltage, allowing for more electrochemical reactions to occur. The reason for the increase in Fe corrosion with increasing pulse width can be explained by the amount of time the electrode is exposed to

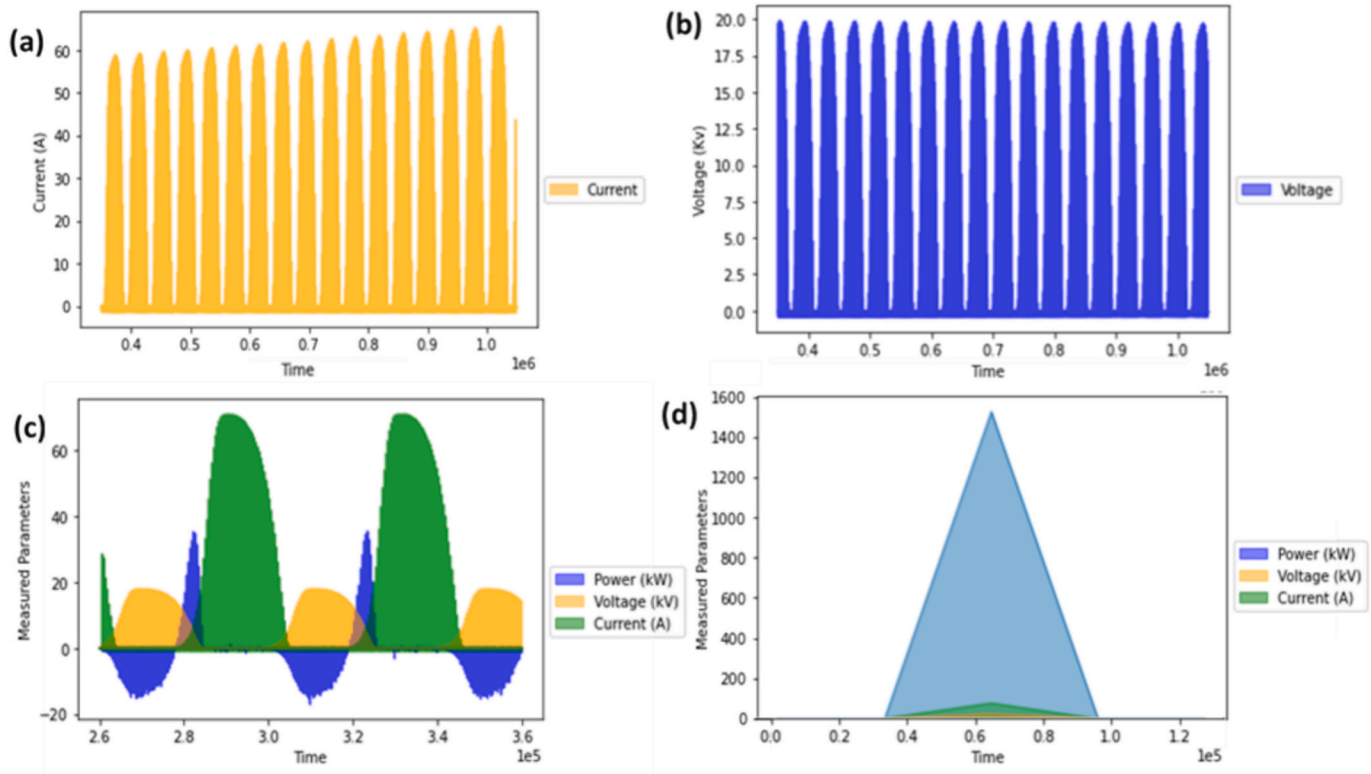


**Fig. 4.** (A) the current waveform during a single PEF run. (B) the voltage waveform during a single PEF run. (C) the current, voltage and power waveform for a 100 Hz run. (D) the current, voltage and power waveform for a 1 Hz run.

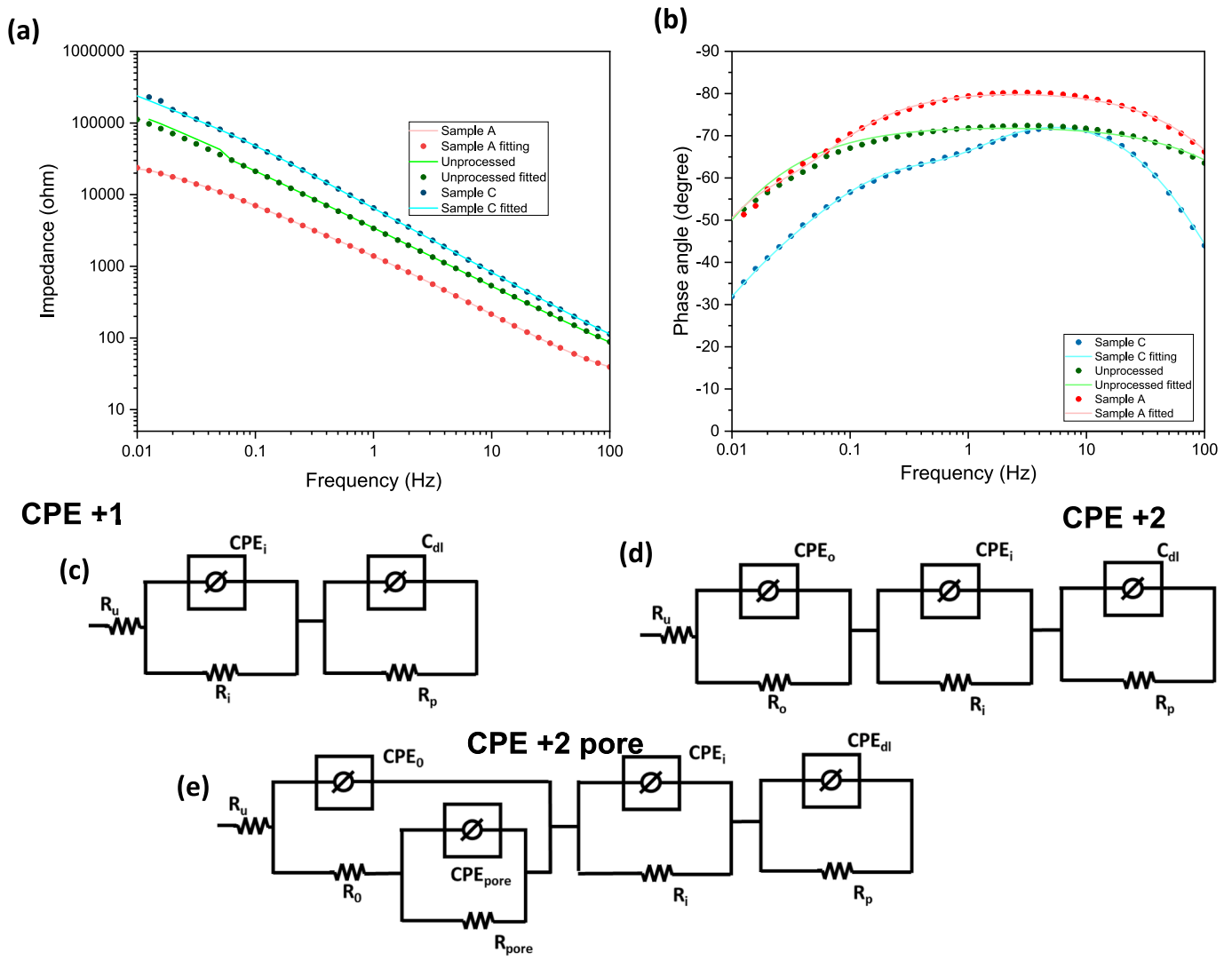


**Fig. 5.** Electrochemical impedance plots for laser processed samples (a) Bode impedance plot (b) Bode phase plot, (c) EEC for unprocessed (CPE + 1), (d) EEC for S-A (CPE + 2), and (e) EEC for S-C (CPE + 2 pore).

voltages above the threshold voltage. As shown in Fig. 3 the increased pulse width has a significant impact on the total energy applied to the system. Because the peak voltage remains relatively constant during the run, this total energy increase may be observed as an increase in current density (A/cm$^2$) across the system. In order to minimize the time that it takes to reach the threshold voltage, the current density must be increased. This will allow for a greater portion of the pulse length to be above the threshold voltage, increasing corrosion on the system. When the voltage is raised, the cause for increased corrosion is due to the larger applied over potential, which allows more voltage to be applied to the electrode, resulting in electrochemical reactions on the electrode surface.

Nickel follows the same trend as Iron for metal ions released, while chromium and manganese have been reduced to a two-factor model with an extremely small pulse width dependence compared to Iron, which could be explained by the lower concentration of both elements in solution and the lower range of values available for pulse width in the system.

### 4.2. Waveform

The current and voltage waveforms are in phase at low frequencies. This demonstrates that the interface impedance is essentially resistive. Hence, when the frequency is low, in the equivalent circuit model, the capacitor's impedance magnitude is high, so most current flows through the resistor. Lowering the frequency while maintaining the same peak-to-peak voltage causes an increase in charge and thus an increase in voltage at the double layer, allowing more electrochemical reactions to occur (Schulz, 2010).

When the waveforms are out of phase, the impedance is not purely resistive, causing the circuit to be dependent also on the capacitance of the double layer. Absolute dielectric constant and absolute dielectric loss would both be noticeable at higher frequencies. This modification causes in a similar way to an alternating current circuit. As the frequency rises, more current flows to the capacitor and less through the rest of the circuit, allowing for less charge build up on the capacitor and thus reducing electrochemical reactions (Schulz, 2010). The phase change observed at the two frequencies remains constant throughout the running process this was seen by the constant Lissojous curve.

The EIS graphs indicate that the phase shift and impedance varies for each sample, with sample S-A demonstrating consistently lower impedance across the entire test range. This reduced impedance corresponds to a greater phase shift within the circuit, causing the electrode to behave more like a capacitor and displaying more pronounced AC circuit characteristics.

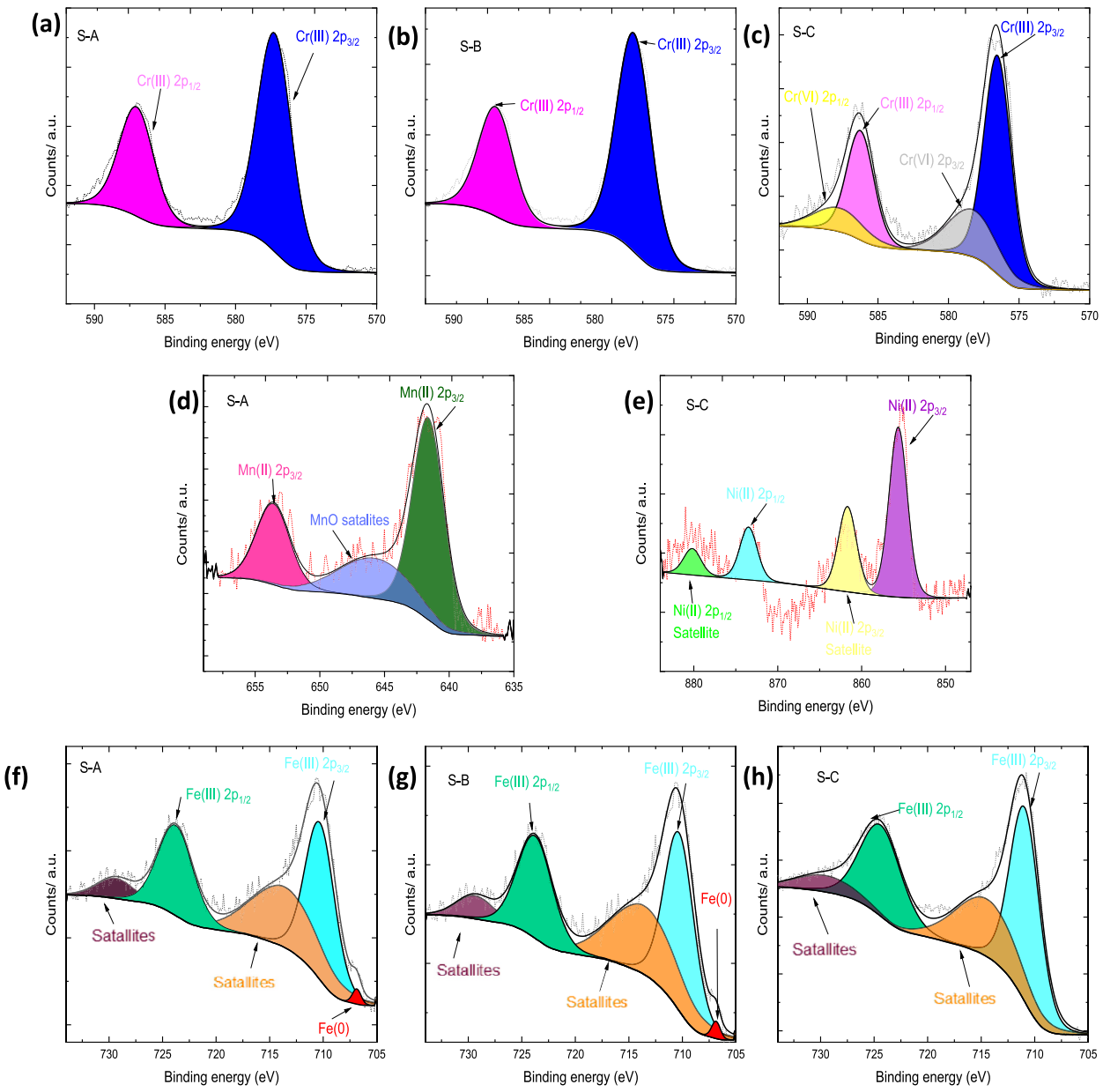


**Fig. 6.** High-resolution XPS spectra of (a) Cr 2p for S-A, (b) Cr 2p for S-B, (c) Cr 2p for S-C, (d) Mn 2p for S-A, (e) Ni 2p for S-C, (f) Fe 2p for S-A, (g) Fe 2p for S-B, (h) Fe 2p for S-C.

### *4.3. XPS*

XPS analysis of the surfaces show that the laser areal energy plays a vital role in determining the surface chemistry. For instance, both S-A and S-B samples processed with a similar areal laser energy at ~1.25 × $10^{24}$ J/cm$^2$ exhibit an oxide layer with a high Cr/Fe ratio of 3.61 and 2.63 respectively. This is expected to increase the general corrosion observed for both samples. S-C was processed with a higher laser density of 8.39 × $10^{24}$ J/cm$^2$, which correlates with the lower Cr/Fe ratio of 0.25. These observations can be explained by the thermo-kinetic model developed by Cui et al., 2014 where chromium is oxidized during the initial exposure to the laser source due to it higher oxygen affinity. This chromium rich layer is then preserved on the surface due to the non-equilibrium oxidation experience due to the rapid heating and cooling of laser processing which does not facilitate diffusion of other elements at lower areal energy. When higher energy is used, longer diffusion times increase the Fe concentration on the surface due to its higher bulk concentration and higher ion mobility inside the oxide film this intern suppresses the Cr concentration on the surface and increase Fe and other allowing elements.

### *4.4. Reduced metal released*

It can be seen from Fig. 7 that the concentration of elemental ions released after PEF processing is reduced for all the laser processed samples with all samples taking 3 times as many pulses to surpass the metals released from unprocessed after 10,000 pulses. With S-A and S-B preforming slightly better than S-C after 30,000 pulses having 28.47, 28.98 and 42.73 ppb total ions respectively. This shows that all the laser processing conditions have a positive effect on the metal released. When you look into the individual elements you can see that the total metal released are made up of vastly different elemental composition. The S-C sample does not produce a concentration of ions higher than that of the unprocessed stainless steel sample for any of the elements after 10,000 pulses. While for S-A (0.60 ppb) and S-B (0.55 ppb) samples, the Cr concentration exceeds that of the unprocessed SS (0.18 ppb) after

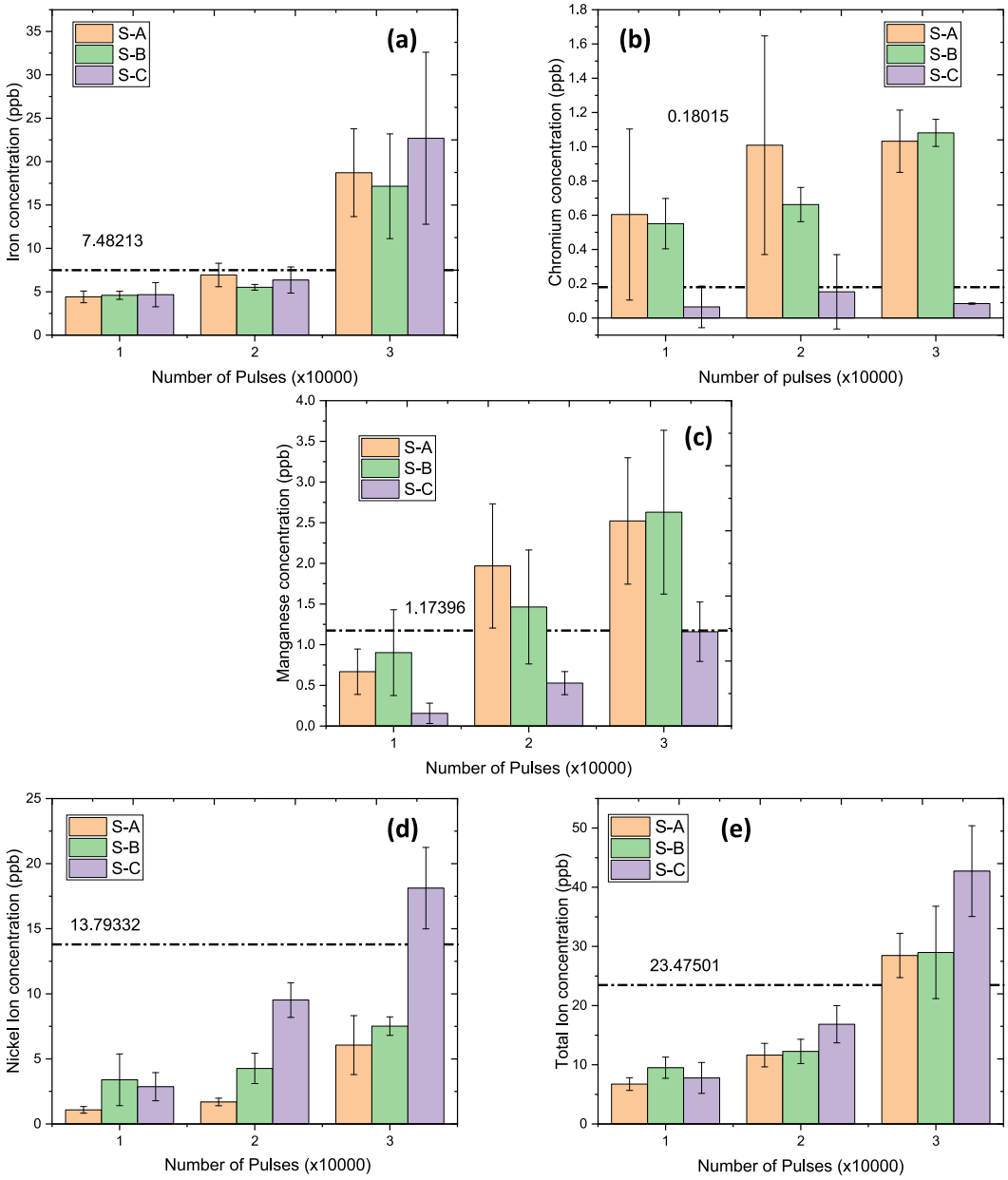


**Fig. 7.** Metal ion concentration vs number of pulses for (a) Fe ion concentration, (b) Cr ion concentration, (c) Mn ion concentration, (d) Ni ion concentration, (E) Total ion concentration. With black line representing the ion concentration at 10000 pulses for unprocessed stainless steel.

10,000 pulses. While for nickel, S-C (18.12 ppb) experiences a lot higher Ni leaching than S-A (6.06 ppb) and S-B (7.52 ppb) after 30,000 pulses. This alteration in leaching concentrations can be explained by the respective surface compositions of the samples with S-A and S-B both exhibiting higher Cr and Mn concentrations, while S-C contains more Ni. The reason for a higher Ni concentration in solution compared to that of Cr, even with a lower surface composition, is due to Ni lower reaction potential compared to Cr, (−0.2 V and − 0.41 V respectively, this allows for electrochemical reactions to take place at a lower potential for Ni than Cr (Roodenburg et al., 2005b). This alteration in surface chemistry allows for the selective reduction of elements in the processing solution.

### 4.5. *Selective reduction of elements*

Excess amounts of nickel and chromium have been seen to cause negative health effects in humans such as in contact dermatitis, cardiovascular disease, asthma, lung fibrosis, and even respiratory system cancers which is especially seen for Cr(VI) exposure(Chen et al., 2017; Deng et al., 2019; Genchi et al., 2020). Human exposure to these elements has been seen to come from a variety of sources such as soils, water, plants and animals. While there is no known human enzymes or cofactors dependent on Ni for normal function, Cr(III) is essential for human health and metabolism of glucose, protein and fat; however, excess amounts of both can cause adverse effects (Genchi et al., 2020; Wilbur et al., 2012). Thus, the reduction of exposure to these elements is important. The US average daily exposure for Ni and Cr at 162 μg and 76 μg respectively (TR) (Trumbo et al., 2001). The FDA advised Tolerable Upper Intake Level (UL) is 1000 μg for Ni and 120 μg for Cr. This shows that the daily exposure to Cr is nearly at the UL, and for individuals with metal sensitivities, the levels are even more concerning (Wilbur et al., 2012). Laser processing therefore can reduce the concentration of individual elements, while also reducing the overall corrosion of the electrodes. This can be particularly useful for food products such as peanuts, peas and chocolate milk which have a high nickel content

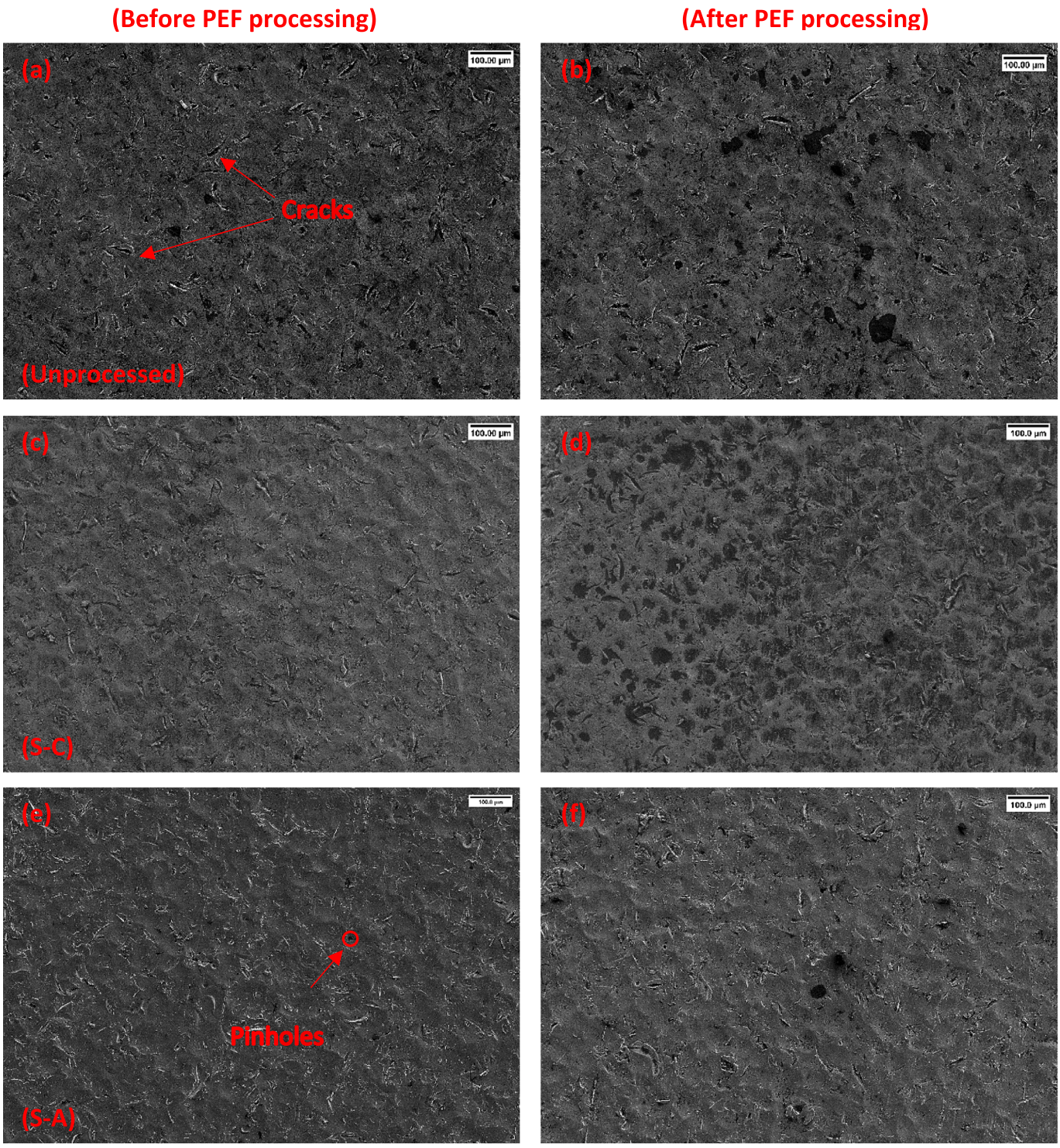


**Fig. 8.** SEM images of 316 L stainless steel under various conditions: (a) unprocessed before PEF treatment, (b) unprocessed after PEF treatment, (c) S-C condition before PEF treatment, (d) S-C condition after PEF treatment, (e) S-A condition before PEF treatment, and (f) S-A condition after PEF treatment, see Table 1.

already, close to the UL, at 956 µg/kg, 699 µg/kg and 871 µg/kg respectively (Capar & Cunningham, 2000). Released metal ions can also produce secondary compounds that can have degradation effects on the food product themselves such as the production of OH and OOH radicals from the Fenton reaction of iron ions. These radicals can react with fatty acids and form lipid hydroperoxides and regeneration of another radical. Lipid peroxidised can then produce compounds such as malanoaldehyde and isoprotanes, which have been seen to cause diseases such as neuro generative diseases and diabetes (Lobo et al., 2010).

## 5. Conclusion

The quest for sustainable food processing technologies that maintain and enhance food quality while preserving nutritional value has led to an increased interest in nonthermal methods like pulsed electric fields (PEF). While PEF offers significant advantages such as preserving freshness and reducing energy consumption compared to thermal pasteurisation, it faces challenges like electrode corrosion and biofouling, hindering its widespread adoption in the food industry.

This study presents a novel approach to reducing metal ion release during pulsed electric field (PEF) processing, through the use of laser-induced oxidation of the electrodes. The implementation of this method marks a significant advancement in the field, as it addresses the issue of metal ion release at its source, offering a practical solution to mitigate environmental and health concerns associated with metal contamination.

Whilst the experimental conditions are not fully aligned with industrial PEF settings, e.g. lower field strength but higher total energy input have been applied, The findings reveal the intricate relationship between pulse waveform characteristics, such as frequency and pulse width, and the resulting metal ion release. Notably, the study demonstrates how variations in waveform parameters influence the electrochemical reactions at the electrode interface, affecting the corrosion behaviour of the system. Furthermore, X-ray photoelectron spectroscopy (XPS) analysis provides valuable insights into the surface chemistry of the processed samples, shedding light on the mechanisms underlying the observed reduction in metal ion release. In the future, additional experiments should be conducted in real-time food processing environments to assess the potential for biofouling and corrosion.

The optimized results indicate a significant three-time reduction in metal ion release following PEF processing, with the laser-processed samples exhibiting improved performance compared to unprocessed stainless steel. This reduction in metal ion release is attributed to the selective alteration of the surface chemistry mainly through the increased Cr/Fe ratio on the surface, resulting in lower concentrations of harmful elements such as nickel and chromium. Given the adverse health effects associated with exposure to these elements, particularly in food products, the selective reduction achieved through PEF processing holds considerable promise for enhancing food safety and quality while also increasing the life time of the electrodes.

Overall, the findings highlight the potential of laser-induced oxidation as a practical solution for enhancing PEF electrode performance and reducing metal ion release in food processing applications. This method provides a solution for overcoming these obstacles and advancing the field of nonthermal food processing. By addressing key challenges in PEF technology, such as electrode corrosion and PEF parameter optimisation, this research contributes to the advancement of sustainable food processing methods with broader implications for food safety and human health. Thus, this innovative technique of laser surface oxidation presents an opportunity to extend the operational lifespan of PEF systems while maintaining or even enhancing processing efficiency and product quality.

## Author agreement statement

We the undersigned declare that this manuscript is original, has not been published before and is not currently being considered for publication elsewhere.

We confirm that the manuscript has been read and approved by all named authors and that there are no other persons who satisfied the criteria for authorship but are not listed. We further confirm that the order of authors listed in the manuscript has been approved by all of us.

We understand that the Corresponding Author is the sole contact for the Editorial process. He/she is responsible for communicating with the other authors about progress, submissions of revisions and final approval of proofs.

## Funding

This publication has emanated from research supported by a research grant from Science Foundation Ireland (SFI) under Grant numbers 18/EPSRC-CDT/3584 and 16/RC/3872 and is co-funded under the European Regional Development Fund.

## CRediT authorship contribution statement

Mark Swayne: Conceptualization, Methodology, Software, Data curation, writing – original draft, Visualization, Investigation, Formal analysis, Writing – review & editing. Dermot Brabazon: Conceptualization, Validation, Resources, Writing – review & editing, Supervision, Project administration, funding acquisition. Gopinath Perumal: Formal analysis, Writing – review & editing. Davide Mariotti: Data analysis for XPS, review and editing, funding for XPS and XPS measurements. Dilli Babu Padmanaban: Data curation for XPS, Data analysis for XPS, review and editing

## Declaration of competing interest

The authors declare the following financial interests/personal relationships which may be considered as potential competing interests:

Mark Swayne reports financial support was provided by Dublin City University. If there are other authors, they declare that they have no known competing financial interests or personal relationships that could have appeared to influence the work reported in this paper.

## Data availability

Data will be made available on request.

## Acknowledgements

This publication has emanated from research supported in part by a grant from Science Foundation Ireland under Grant numbers 18/EPSRC-CDT/3584 and 16/RC/3872, our industry partner PRO Stainless Ltd., Ireland, and is co-funded under the European Regional Development Fund. The processing vessel was supplied by ELEA technology gmbh. For the purpose of Open Access, the author has applied a CC BY public copyright licence to any Author Accepted Manuscript version arising from this submission. The work was also partially supported by EPSRC award EP/R008841/1.

## Appendix A. Supplementary data

Supplementary data to this article can be found online at https://doi.org/10.1016/j.ifset.2024.103789.

## References

Aadil, R. M., Khalil, A. A., Rehman, A., Khalid, A., Inam-ur-Raheem, M., Karim, A., … Afraz, M. T. (2020). Assessing the impact of ultra-sonication and thermo-ultrasound on antioxidant indices and polyphenolic profile of apple-grape juice blend. *Journal of Food Processing and Preservation, 44*(5). https://doi.org/10.1111/jfpp.14406

Aadil, R. M., Zeng, X., Han, Z., Sahar, A., Khalil, A. A., Rahman, U. U., … Mehmood, T. (2018). Combined effects of pulsed electric field and ultrasound on bioactive compounds and microbial quality of grapefruit juice. *Journal of Food Processing and Preservation, 42*(2), Article e13507. https://doi.org/10.1111/jfpp.13507

Aadil, R. M., Zeng, X.-A., Ali, A., Zeng, F., Farooq, M. A., Han, Z., … Jabbar, S. (2015). Influence of different pulsed electric field strengths on the quality of the grapefruit juice. *International Journal of Food Science & Technology, 50*(10), 2290–2296. https://doi.org/10.1111/ijfs.12891

Ahmed Obeidi, M., McCarthy, E., Ubani, S. I., Ul Ahad, I., & Brabazon, D. (2019). Effect of surface roughness on $CO_2$ laser absorption by 316L stainless steel and aluminum. *Materials Performance and Characterization, 8*(6), 1167–1177. https://doi.org/10.1520/MPC20180091

Alda, J. (2003). *Laser and Gaussian Beam propagation and transformation*. Encyclopedia of Optical Engineering. https://doi.org/10.1081/E-EOE 120009751

Ashokkumar, S., & Adler-Nissen, J. (2011). Evaluating non-stick properties of different surface materials for contact frying. *Journal of Food Engineering, 105*(3), 537–544. https://doi.org/10.1016/j.jfoodeng.2011.03.018

Capar, S. G., & Cunningham, W. C. (2000). Element and radionuclide concentrations in food: FDA Total diet study 1991–1996. *Journal of AOAC International, 83*(1), 157–177. https://doi.org/10.1093/jaoac/83.1.157

Chen, Q. Y., Brocato, J., Laulicht, F., & Costa, M. (2017). *Essential and non-essential metals, molecular and integrative toxicology*. NY, USA: Springer New York.

Cui, C. Y., Cui, X. G., Ren, X. D., Qi, M. J., Hu, J. D., & Wang, Y. M. (2014). Surface oxidation phenomenon and mechanism of AISI 304 stainless steel induced by Nd:

YAG pulsed laser. *Applied Surface Science, 305*, 817–824. https://doi.org/10.1016/j.apsusc.2014.04.025

Deng, Y., Wang, M., Tian, T., Lin, S., Xu, P., Zhou, L., … Dai, Z. (2019). The effect of hexavalent chromium on the incidence and mortality of human cancers: a meta-analysis based on published epidemiological cohort studies. *Frontiers in Oncology, 9*, 24. https://doi.org/10.3389/fonc.2019.00024

Gad, A., Jayaram, S. H., & Pritzker, M. (2014). Performance of electrode materials during food processing by pulsed electric fields. *IEEE Transactions on Plasma Science, 42*(10), 3161–3166. https://doi.org/10.1109/TPS.2014.2312711

Gášková, D., Sigler, K., Janderová, B., & Plášek, J. (1996). Effect of high-voltage electric pulses on yeast cells: Factors influencing the killing efficiency. *Bioelectrochemistry and Bioenergetics, 39*(2), 195–202. https://doi.org/10.1016/0302-4598(95)01892-1

Gavahian, M., Chu, Y.-H., & Sastry, S. (2018). Extraction from food and natural products by moderate electric field: Mechanisms, benefits, and potential industrial applications. *Comprehensive Reviews in Food Science and Food Safety, 17*(4), 1040–1052. https://doi.org/10.1111/1541-4337.12362

Genchi, G., Carocci, A., Lauria, G., Sinicropi, M. S., & Catalano, A. (2020). Nickel: Human health and environmental toxicology. *International Journal of Environmental Research and Public Health, 17*(3). https://doi.org/10.3390/ijerph17030679

Góngora-Nieto, M. M., Sepúlveda, D. R., Pedrow, P., Barbosa-Cánovas, G. V., & Swanson, B. G. (2002). Food processing by pulsed electric fields: Treatment delivery, inactivation level, and regulatory aspects. *LWT - Food Science and Technology, 35*(5), 375–388. https://doi.org/10.1006/fstl.2001.0880

Kotnik, T., Miklavčič, D., & Mir, L. M. (2001). Cell membrane electropermeabilization by symmetrical bipolar rectangular pulses. *Bioelectrochemistry, 54*(1), 91–95. https://doi.org/10.1016/S1567-5394(01)00115-3

Łęcka, K. M., Antończak, A. J., Szubzda, B., Wójcik, M. R., Stępak, B. D., Szymczyk, P., … Abramski, K. M. (2016). Effects of laser-induced oxidation on the corrosion resistance of AISI 304 stainless steel. *Journal of Laser Applications, 28*(3), 32009. https://doi.org/10.2351/1.4948726

Li, X., & Farid, M. (2016). A review on recent development in non-conventional food sterilization technologies. *Journal of Food Engineering, 182*, 33–45. https://doi.org/10.1016/j.jfoodeng.2016.02.026

Li, Z. L., Zheng, H. Y., Teh, K. M., Liu, Y. C., Lim, G. C., Seng, H. L., & Yakovlev, N. L. (2009). Analysis of oxide formation induced by UV laser coloration of stainless steel. *Applied Surface Science, 256*(5), 1582–1588. https://doi.org/10.1016/j.apsusc.2009.09.025

Lobo, V., Patil, A., Phatak, A., & Chandra, N. (2010). Free radicals, antioxidants and functional foods: Impact on human health. *Pharmacognosy Reviews, 4*(8), 118–126. https://doi.org/10.4103/0973-7847.70902

Lu, Y., Shi, X., Huang, Z., Li, T., Zhang, M., Czajkowski, J., Fabritius, T., Huttula, M., & Cao, W. (2017). Nanosecond laser coloration on stainless steel surface. *Scientific Reports, 7*(1), 7092. https://doi.org/10.1038/s41598-017-07373-8

Matra, K., Buppan, P., & Techaumnat, B. (2020). Analytical and experimental studies on the application of a series of treatment chambers for *Escherichia coli* inactivation by pulsed electric fields. *Applied Sciences, 10*(12), 4071. https://doi.org/10.3390/app10124071

Meneses, N., Jaeger, H., & Knorr, D. (2011). pH-changes during pulsed electric field treatments — Numerical simulation and in situ impact on polyphenoloxidase inactivation. *Innovative Food Science & Emerging Technologies, 12*(4), 499–504. https://doi.org/10.1016/j.ifset.2011.07.001

Nowosad, K., Sujka, M., Pankiewicz, U., & Kowalski, R. (2021). The application of PEF technology in food processing and human nutrition. *Journal of Food Science and Technology, 58*(2), 397–411. https://doi.org/10.1007/s13197-020-04512-4

Pataro, G., & Ferrari, G. (2022). *Electrochemical reactions in pulsed electric fields treatment* (pp. 143–166). https://doi.org/10.1007/978-3-030-70586-2_4

Rodaitė-Riševičienė, R., Saulė, R., Snitka, V., & Saulis, G. (2014). Release of Iron ions from the stainless steel anode occurring during high-voltage pulses and its consequences for cell electroporation technology. *IEEE Transactions on Plasma Science, 42*(1), 249–254. https://doi.org/10.1109/TPS.2013.2287499

Roodenburg, B., de Haan, S. W. H., van Boxtel, L. B. J., Hatt, V., Wouters, P. C., Coronel, P., & Ferreira, J. A. (2010). Conductive plastic film electrodes for pulsed electric field (PEF) treatment—A proof of principle. *Innovative Food Science & Emerging Technologies, 11*(2), 274–282. https://doi.org/10.1016/j.ifset.2010.01.005

Roodenburg, B., Morren, J., Berg, H. E. I., & de Haan, S. W. H. (2005a). Metal release in a stainless steel pulsed electric field (PEF) system. *Innovative Food Science & Emerging Technologies, 6*(3), 337–345. https://doi.org/10.1016/j.ifset.2005.04.004

Roodenburg, B., Morren, J., Berg, H. E. I., & de Haan, S. W. H. (2005b). Metal release in a stainless steel pulsed electric field (PEF) system. *Innovative Food Science & Emerging Technologies, 6*(3), 327–336. https://doi.org/10.1016/j.ifset.2005.04.006

Sale, A., & Hamilton, W. (1967). Effects of high electric fields on microorganismsI. Killing of bacteria and yeasts. *Biochimica et Biophysica Acta (BBA) - General Subjects, 148*(3), 781–788. https://doi.org/10.1016/0304-4165(67)90052-9

Samaranayake, C. P., & Sastry, S. K. (2005). Electrode and pH effects on electrochemical reactions during ohmic heating. *Journal of Electroanalytical Chemistry, 577*(1), 125–135. https://doi.org/10.1016/j.jelechem.2004.11.026

Schulz, A. L. (2010). *Capacitors: Theory, types and applications*. Nova Science Publishers, Incorporated. https://books.google.ie/books?id=TcwPRQAACAAJ.

Swayne, M., Perumal, G., & Brabazon, D. (2024). Mechanism for control of laser-induced stainless steel oxidation. *Advanced Materials Interfaces, 11*(17), 2300991. https://doi.org/10.1002/admi.202300991

Tanino, T., Hirosawa, M., Moteki, R., Matsui, M., & Ohshima, T. (2020). Engineering of pulsed electric field treatment using carbon materials as electrode and application to pasteurization of sake. *Journal of Electrostatics, 104*, Article 103424. https://doi.org/10.1016/j.elstat.2020.103424

Trumbo, P., Yates, A. A., Schlicker, S., & Poos, M. (2001). Dietary reference intakes: Vitamin a, vitamin K, arsenic, boron, chromium, copper, iodine, iron, manganese, molybdenum, nickel, silicon, vanadium, and zinc. *Journal of the American Dietetic Association, 101*(3), 294–301. https://doi.org/10.1016/S0002-8223(01)00078-5

Tsong, T. Y. (1991). Electroporation of cell membranes. *Biophysical Journal, 60*(2), 297–306. https://doi.org/10.1016/S0006-3495(91)82054-9

Tylewicz, U. (2020). How does pulsed electric field work?. In *Pulsed electric fields to obtain healthier and sustainable food for tomorrow* (pp. 3–21). Elsevier. https://doi.org/10.1016/B978-0-12-816402-0.00001-X.

Wilbur, S., Abadin, H., Fay, M., Yu, D., Tencza, B., Ingerman, L., … James, S. (2012). *Toxicological profile for chromium*.

Yogesh, K. (2016). Pulsed electric field processing of egg products: A review. *Journal of Food Science and Technology, 53*(2), 934–945. https://doi.org/10.1007/s13197-015-2061-3

Zhang, C., Lyu, X., Arshad, R. N., Aadil, R. M., Tong, Y., Zhao, W., & Yang, R. (2023). Pulsed electric field as a promising technology for solid foods processing: A review. *Food Chemistry, 403*, Article 134367. https://doi.org/10.1016/j.foodchem.2022.134367

Zhao, W., Yang, R., Lu, R., Wang, M., Qian, P., & Yang, W. (2008). Effect of PEF on microbial inactivation and physical–chemical properties of green tea extracts. *LWT - Food Science and Technology, 41*(3), 425–431. https://doi.org/10.1016/j.lwt.2007.03.020